# Searching for the nuclear liquid-gas phase transition in Au+Au collisions at 35 MeV/nucleon

M. Belkacem,[1,2,*] P. F. Mastinu,[1,3] V. Latora,[2] A. Bonasera,[2] M. D'Agostino,[1] M. Bruno,[1] J. D. Dinius,[4] M. L. Fiandri,[1] F. Gramegna,[5] D. O. Handzy,[4] W. C. Hsi,[4] M. Huang,[4] G. V. Margagliotti,[6] P. M. Milazzo,[6] C. P. Montoya,[4] G. F. Peaslee,[4] R. Rui,[6] C. Schwarz,[4] G. Vannini,[6] and C. Williams[4]

[1]*Dipartimento di Fisica and INFN, Bologna, Italy*

[2]*INFN, Laboratorio Nazionale del Sud, Catania, Italy*

[3]*Dipartimento di Fisica, Padova, Italy*

[4]*National Superconducting Cyclotron Laboratory, Michigan State University, East Lansing, Michigan 48824*

[5]*INFN, Laboratori Nazionali di Legnaro, Italy*

[6]*Dipartimento di Fisica and INFN, Trieste, Italy*

(Received 17 April 1996)

Within the framework of classical molecular dynamics, we study the collision Au+Au at an incident energy of 35 MeV/nucleon. It is found that the system shows a critical behavior at peripheral impact parameters, revealed through the analysis of conditional moments of charge distributions, Campi scatter plot, and the occurrence of large fluctuations in the region of the Campi plot where this critical behavior is expected. When applying the experimental filters of the MULTICS-MINIBALL apparatus, it is found that criticality signals can be hidden due to the inefficiency of the experimental apparatus. The signals are recovered by identifying semiperipheral and peripheral collisions looking to the velocity distribution of the largest fragment, and selecting the most complete events. [S0556-2813(96)01811-0]

PACS number(s): 25.70.Mn, 05.70.Fh, 21.65.+f, 64.70.Fx

## I. INTRODUCTION

For several years, the idea that nuclear systems may show some evidence for the occurrence of critical behavior related to a liquid-gas phase transition has stimulated lots of investigations both from theoretical and experimental sides [1–8]. This was suggested more than ten years ago by the observation of fragment charge distributions exhibiting power laws [9]. Such a power law is expected for cluster formation near the critical point of a liquid-gas phase transition, as in the Fisher droplet model [10]. This interest increased recently with the determination by the EOS Collaboration of critical exponents of fragmenting nuclear systems produced in the collision of 1 GeV/nucleon Au nuclei with a carbon target [11], and with the extraction by the ALADIN Collaboration of a caloric curve resulting from the fragmentation of the quasiprojectile formed in the collision Au+Au at 600 MeV/nucleon, reminiscent of the behavior of a liquid-gas system [12].

In the present work, we study within the framework of classical molecular dynamics (CMD) model, the reaction $^{197}$Au + $^{197}$Au at an incident energy of 35 MeV/nucleon. We analyze the results in terms of critical behavior by studying fragment charge distributions, their moments, and the occurrence of large fluctuations in terms of intermittency analysis, and as shown by the fluctuations of the size of the largest fragment. Our aim for this analysis is threefold. First, critical behavior has been observed in the fragmentation of Au nuclei in the previously mentioned experiments at high beam energies (600 and 1000 MeV/nucleon), and we are interested to see if such a behavior can still be observed at an energy notably lower. Second, we want to identify the critical events (if any) and study the effects of the efficiency of experimental apparatus (by applying for example the experimental filters of the MULTICS-MINIBALL apparatus [13,14]). From this we can see whether experimental inefficiencies can completely wash out the signals of criticality or if it is still possible to recover these signals from the filtered results. Finally, we aim to apply the same procedure to the experimental data obtained by the MULTICS-MINIBALL collaboration for the same reaction [15].

This paper is organized as follows. We give in Sec. II a brief description of the CMD model used for this study. A more complete description can be found in Refs. [16,17]. Section III contains the analysis of the moments of charge distributions, the Campi scatter plot, and the analysis of the scaled factorial moments in terms of the intermittency signal. Section IV is devoted to the study of the effects of experimental inefficiencies, applying to the CMD results the filter of the MULTICS-MINIBALL apparatus, and we show it is possible to recover the signals of criticality selecting well detected events. Finally, we give in Sec. V our summary and conclusions.

## II. BRIEF DESCRIPTION OF THE CMD MODEL

In the CMD model, we assume that each nucleus is made up of 197 nucleons (79 protons + 118 neutrons) that move under the influence of a two-body potential $V$ consisting of two different interactions [16]:

$$V_{nn}(r)=V_{pp}(r)=V_0[\exp(-\mu_0 r)/r-\exp(-\mu_0 r_c)/r_c],$$

$$V_{np}(r)=V_r[\exp(-\mu_r r)/r-\exp(-\mu_r r_c)/r_c] - V_a[\exp(-\mu_a r)/r-\exp(-\mu_a r_a)/r_a]. \quad (1)$$

*Present address: Institut für Theoretische Physik, J. W. Goethe-Universität, D-60054 Frankfurt am Main, Germany.

 

$r_c = 5.4$ fm is a cutoff radius. The first interaction, for identical nucleons, is purely repulsive so no bound state of identical nucleons can exist (to simulate in some sense the Pauli principle), and the second, for proton-neutron interaction, is attractive at large distances and repulsive at small ones [16]. The various parameters entering Eq. (1) are defined with their respective values in Ref. [16]. This potential gives an equation of state (EOS) of classical matter having about 250 MeV of compressibility (set *M* in Ref. [16]), and which strikingly resembles that of nuclear matter [i.e., equilibrium density $\rho_0 = 0.16$ fm$^{-3}$ and energy $E(\rho_0) = -16$ MeV/nucleon]. Furthermore, in Refs. [16,18], it is shown that many experimental data on heavy-ion collisions are reasonably explained by this classical model. Of course this is not accidental but it is due to the accurate choice of the parameters of the two-body potentials [16]. The classical Hamilton's equations of motion are solved using the Taylor method at the order $O[(\delta t)^3]$ where $\delta t$ is the integration time step [19]. Energy and momentum are well conserved. Both nuclei are initialized in their ground state by using the frictional cooling method [20], then they are boosted towards each other with the CM kinetic energy. In the present calculations, the Coulomb interaction is explicitly taken into account. Note that this model takes into account all order correlations at the classical level. This is quite important when studying instabilities.

## III. RESULTS

Calculations for the reaction Au+Au at 35 MeV/nucleon are carried out for several impact parameters, from 1 to 13 fm in steps of 1 fm. One intuitively imagines the following scenario for this reaction. For central collisions, since the incident energy is rather high as compared to the Coulomb barrier, the two heavy nuclei will come in contact for a short time. The total charge of the intermediate system is very high and it will quickly explode due mainly to the high Coulomb repulsion [15]. For increasing impact parameter, two or maybe three excited primary fragments might be formed. By tuning the impact parameter, we might hope to obtain some primary sources which have a combination of excitation energy, Coulomb charge, and angular momentum sufficient to bring the system into the instability region (if any). The possibility that such a scenario might apply to heavy-ion collisions has been shown in microscopic calculations [17,21]. In particular, it has been shown that the ''critical'' excitation energy decreases when the system is either charged and/or rotating [17,21–23]. Thus a combination of all these ingredients might give the desired result. Following this scenario, one would expect to see a critical behavior (if any) for peripheral collisions.

In Fig. 1, we have plotted the dynamical evolution in the *x*-*z* plane for this reaction for four different times (after the two nuclei came in contact), and four different impact parameters; $\hat{b} = 0.15$ (first line panels), $\hat{b} = 0.38$ (second line panels), $\hat{b} = 0.62$ (third line panels), and $\hat{b} = 0.85$ (fourth line panels). For central and semicentral collisions (first and second rows) the two nuclei come in contact with each other and form a unique deformed source (the source is less deformed for more central collisions) which decays through light particles and fragments emission [15]. For semiperipheral and peripheral collisions (third and fourth lines panels), one sees clearly the formation of two big sources (the quasitarget and quasiprojectile) with the formation between them of a third smaller source in the neck region. The size of this ''neck'' is smaller for more peripheral collisions and it completely disappears for the most peripheral ones.

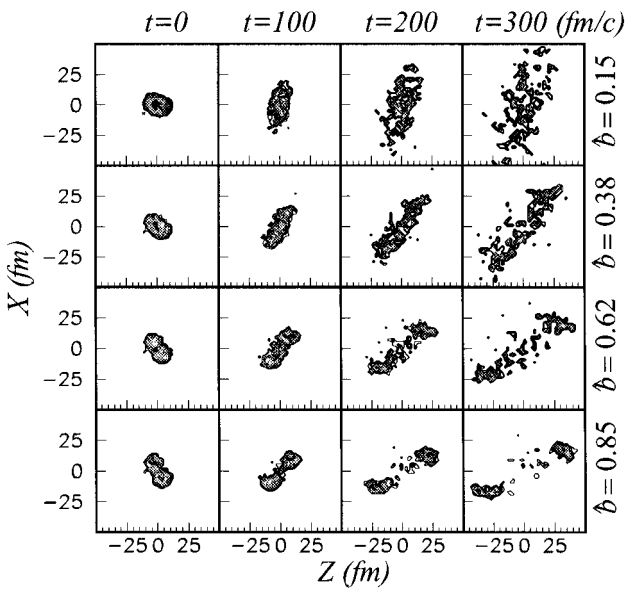


FIG. 1. Dynamical evolution. The *r*-space distribution is projected on the *x*-*z* plane.

One of the most powerful methods used to characterize the critical behavior of a system undergoing a multifragmentation is the method of conditional moments introduced by Campi [24]. The moments of asymptotic cluster charge distributions are defined as

$$m_k^{(j)} = \sum_Z Z^k n^{(j)}(Z)/Z_{\rm tot}, \tag{2}$$

where $n^{(j)}(Z)$ is the multiplicity of clusters of charge $Z$ in the event $j$, $Z_{\rm tot} = 158$, and the sum is over all the fragments in the event *except the heaviest one*, which corresponds to the bulk liquid in an infinite system. If the system keeps some trace of the phase transition for some particular events, the moments $m_k$ should show some strong correlations between them [24]. In particular, the second moment $m_2$, which in macroscopic thermal systems is proportional to the isothermal compressibility, diverges at the critical temperature [11,25,26]. Of course in finite systems, the moments $m_k$ remain finite due to finite size effects. In the upper part of Fig. 2, we have plotted the second moment $m_2$ vs the reduced impact parameter $\hat{b}$, calculated without the two largest fragments instead of the largest one only. This is due to the fact that the system is symmetric, and for peripheral collisions we expect bulk fragments coming from the quasitarget and the quasiprojectile. As expected, the second moment $m_2$ shows a peak for an impact parameter $\hat{b} \approx 0.8$. If we do not take off the second largest fragment (lower part of Fig. 2), we observe a continuous rise of $m_2$ and the peak disappears because we are summing to the small fragments, a very big one (bulk) coming from the fragmenting quasitarget or projectile.

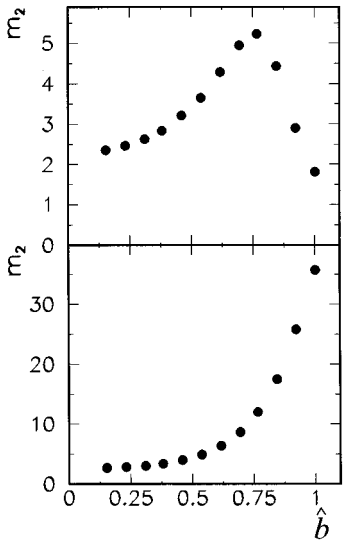


FIG. 2. The second moment of charge distributions $m_2$ vs the reduced impact parameter $\hat{b}$. The upper panel, without the two largest fragments; the lower panel, without only the largest fragment.

In Fig. 3, we have plotted the same quantity $m_2$ vs the multiplicity of charged particles $N_c$ (with $Z \geqslant 1$), calculated without the two largest fragments (upper part) and only without the largest one (lower part). The second moment $m_2$ shows also a peak vs $N_c$ for a multiplicity around 20–25, and this peak disappears when taking into account the second largest fragment. In the following, the analysis of the nonfiltered results is done taking off the two largest fragments.

Another quantity proposed by Campi to give more insight into the critical behavior is the relative variance $\gamma_2$ defined as [24]

$$\gamma_2 = \frac{m_2 m_0}{m_1^2}. \tag{3}$$

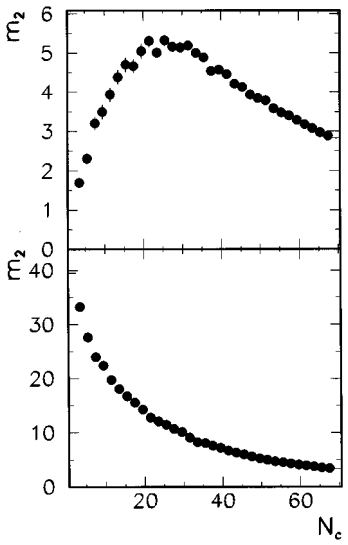


FIG. 3. The second moment of charge distributions $m_2$ vs charged particle multiplicity $N_c$. The upper panel, without the two largest fragments; the lower panel, without only the largest fragment.

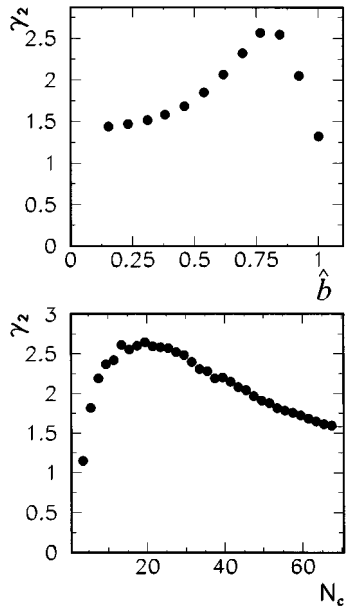


FIG. 4. The reduced variance $\gamma_2$ vs the reduced impact parameter $\hat{b}$ (upper panel) and vs charged particle multiplicity $N_c$ (lower panel). The calculations are done without the two largest fragments.

It was shown by Campi that this quantity presents a peak around the critical point which means that the fluctuations in the fragment size distributions are the largest near the critical point [24]. In Fig. 4, we have plotted the relative variance $\gamma_2$ vs the reduced impact parameter $\hat{b}$ (upper part), and vs the charged particle multiplicity $N_c$ (lower part). One clearly notes that the relative variance $\gamma_2$ shows a peak in both plots, for a reduced impact parameter $\hat{b}$ around 0.8, and for $N_c \approx 20-25$.

Moreover, we have considered another variable which is the normalized variance of the charge of the maximum fragment $\sigma_{\mathrm{NV}}$. As charge distributions are expected to show the maximum fluctuations around the critical point [27], this quantity is expected to present some maximum at the critical point [24,28]. This normalized variance is defined as

$$\sigma_{\mathrm{NV}} = \frac{\sigma^2_{Z_{\max}}}{\langle Z_{\max} \rangle}, \tag{4}$$

where

$$\sigma^2_{Z_{\max}} = \langle Z^2_{\max} \rangle - \langle Z_{\max} \rangle^2. \tag{5}$$

The brackets $\langle\rangle$ indicate an ensemble averaging. We have plotted in Fig. 5 the normalized variance $\sigma_{\mathrm{NV}}$ vs $\hat{b}$ (upper part), and vs $N_c$ (lower part). In this case also, we observe a peak for this quantity in both plots at almost the same values of $\hat{b}$ and $N_c$. This means that the fluctuations in the charge of the maximum fragment (thus in charge distributions) are the largest around these values of the impact parameter and charged particle multiplicity.

The upper part of Fig. 6 shows a scatter plot of $\ln(Z^j_{\max})$ vs $\ln(m^j_2)$ for each event $j$, commonly known as Campi scatter plot. It was shown that if the system keeps some trace of the phase transition, the correlation between these two quan-

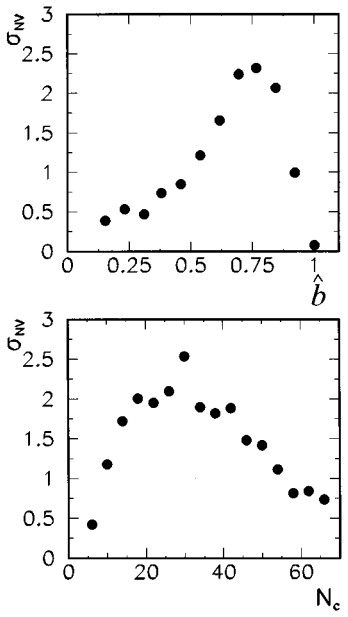


FIG. 5. The normalized variance of the size of the largest fragment $\sigma_{\mathrm{NV}}$ vs the reduced impact parameter $\hat{b}$ (upper panel) and vs charged particle multiplicity $N_c$ (lower panel).

tities exhibits two characteristic branches, an upper branch with an average negative slope corresponding to undercritical events, and a lower branch with a positive slope that corresponds to overcritical events, and the two branches meet close to the critical point of the phase transition [17,24,29]. The results of Fig. 6 show two branches corresponding to undercritical and overcritical events, similar to the predicted ones. Note that the upper branch contains mainly events at impact parameters $\hat{b}>0.85$, while the lower branch contains events with $\hat{b}<0.77$. The region where the two branches meet is obtained for $0.77\leqslant\hat{b}\leqslant0.85$. In the following, we will show that the central region where the two branches meet and where the critical behavior is expected, is characterized by the occurrence of large fluctuations, revealed through an intermittency analysis [30]. In the lower part of Fig. 6, we have plotted the logarithm of the scaled factorial moments (SFM's) defined as [31]

$$F_i(\delta s)=\frac{\sum_{k=1}^{Z_{\mathrm{tot}}/\delta s}\langle n_k\cdot(n_k-1)\cdot\cdots\cdot(n_k-i+1)\rangle}{\sum_{k=1}^{Z_{\mathrm{tot}}/\delta s}\langle n_k\rangle^i}, \quad (6)$$

$i=2,\ldots,5$ vs the logarithm of the bin size $\delta s$. In the above definition of the SFM, $i$ is the order of the moment. The total interval $1-Z_{\mathrm{tot}}$ ($Z_{\mathrm{tot}}=158$) is divided in $M=Z_{\mathrm{tot}}/\delta s$ bins of size $\delta s$, $n_k$ is the number of particles in the $k$th bin for an event, and the brackets $\langle\rangle$ denote the average over many events. An intermittent pattern of fluctuations is characterized by a linear rise of the logarithm of the SFM's vs $-\ln(\delta s)$ (i.e., $F_i\propto\delta s^{-\lambda_i}$) which corresponds to the existence of large fluctuations which have self-similarity over the whole range of scales considered [29–31]. Even though this quantity is ill defined for fragment distributions [32,33], it has been shown in several theoretical studies that critical events give a power law for the SFM vs the bin size [17,18,28,31,34,35]. In the figure, the logarithm of the SFM's exhibits a linear rise vs the logarithm of the bin size indicating a strong intermittency signal in the region of the Campi plot where the critical behavior is expected. To understand whether these large fluctuations are due to a simple event mixing by considering different impact parameters inside cut 2, we fixed the impact parameter to, say $\hat{b}=0.85$. The resulting SFM are shown in Fig. 7. One notes that the signal is still there even though it is much weaker than the previous case, Fig. 6 (the absolute values of the SFM are smaller). This allows us to conclude that the intermittency signal is not due to the mixing of events and this mixing only increases the absolute values of the SFM.

Now we would like to add some comments about the mixing of different sources in the calculations of the quanti-

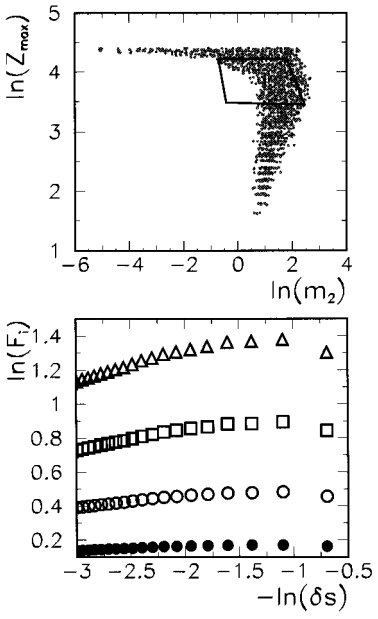


FIG. 6. Upper panel: Campi scatter plot. The logarithm of the size of the largest fragment $\ln(Z_{\mathrm{max}})$ is plotted vs the logarithm of the second moment $\ln(m_2)$. Lower panel: The logarithm of the scaled factorial moments $\ln(F_i)$ is plotted vs the logarithm of the bin size $-\ln(\delta s)$ for the events falling within the cut drawn in the Campi scatter plot, upper panel. Solid circles represent the SFM of order $i=2$, open circles $i=3$, open squares $i=4$, and open triangles $i=5$.

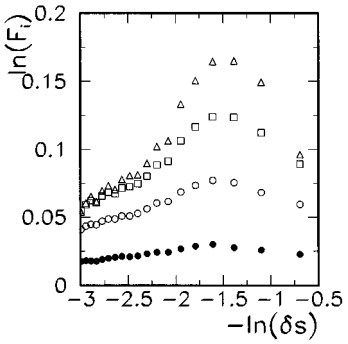


FIG. 7. The logarithm of the scaled factorial moments $\ln(F_i)$ is plotted vs the logarithm of the bin size $-\ln(\delta s)$ for the events with $\hat{b}=0.84$. Solid circles represent the SFM of order $i=2$, open circles $i=3$, open squares $i=4$, and open triangles $i=5$.

ties discussed above. First of all, we note that it is not clear how to separate the different sources which might be formed after the first stages of the collision when they are still overlapping (we mean by overlap distances smaller than the range of the two-body interaction used, i.e., $r_c = 5.4$ fm), as one can see from Fig. 1. Thus it is not obvious how to distinguish which fragments come from which source, even in a simple dynamical model like CMD. For the calculations of the second moment $m_2$ for instance, one should consider only one source (that entering the critical region). For central collisions, only one source is formed and $m_2$ is calculated according to Eq. (2) with $Z_{\rm tot} \approx 158$. For peripheral impact parameters, one should calculate the second moment only from one source (the PLF or TLF assuming two sources), and in this case $Z_{\rm tot}$ should be around 79 (158/2) in Eq. (2). Since we are dealing with a symmetric reaction, we can say that both the PLF and the TLF enter separately the critical region. So calculating $m_2$ using Eq. (2) with $Z_{\rm tot} \approx 158$ is equivalent to calculating it by summing on the fragments coming from only one source and dividing by $Z_{\rm tot} \approx 79$, which gives the same results as those of Fig. 2. This discussion holds for all the moments $m_k$, and thus for the reduced variance $\gamma_2$. For the normalized variance of the charge of the largest fragment, one should be careful to consider the largest fragment coming from only one source (this was not done for the previous calculations of $\sigma_{\rm NV}$). For central collisions, we have only one source, and the results do not change. For peripheral collisions, by considering only the largest fragment with a positive velocity in the center of mass, the obtained peak in $\sigma_{\rm NV}$ is higher than that obtained previously (3.8 instead of 2.4 of Fig. 5). This result is in some sense obvious because we were previously smoothing the fluctuations of the largest fragment on both sources (PLF and TLF). For the Campi plot, we have plotted the logarithm of the size of the largest fragment vs the logarithm of $m_2$ both calculated for the fragments emitted in the forward direction (with $v_{\rm c.m.} \geqslant 0$ to select roughly the PLF source). The obtained results are very similar to those reported in Fig. 6 and making a gate on the central region of the plot, we obtained almost the same SFM with the same absolute values as those reported on the lower part of Fig. 6.

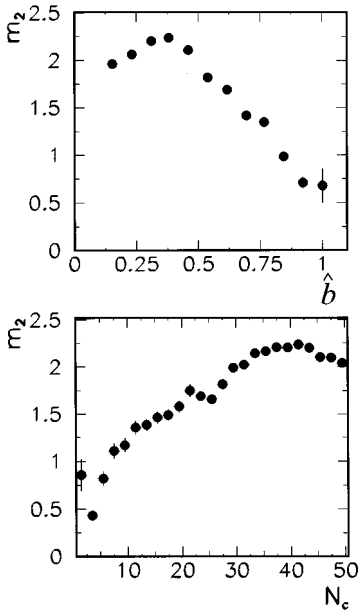


FIG. 8. Filtered CMD results. The second moment of charge distributions $m_2$ vs the reduced impact parameter $\hat{b}$ (upper panel) and vs charged particle multiplicity $N_c$ (lower panel).

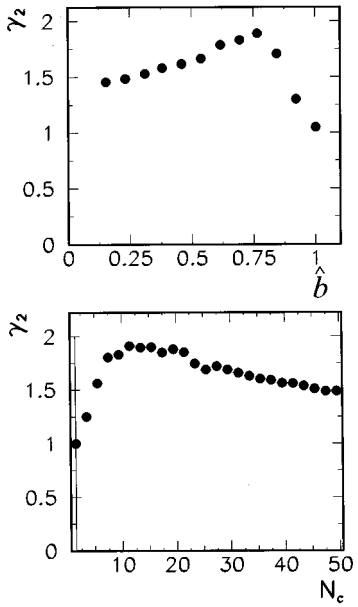


FIG. 9. Filtered CMD results. The reduced variance $\gamma_2$ vs the reduced impact parameter $\hat{b}$ (upper panel) and vs charged particle multiplicity $N_c$ (lower panel).

In this section, we have seen that the analysis of the reaction Au+Au at 35 MeV/nucleon shows a signal of critical behavior in peripheral collisions. This behavior is revealed through the analysis of the second moment of charge distributions, the reduced variance, the large fluctuations of the

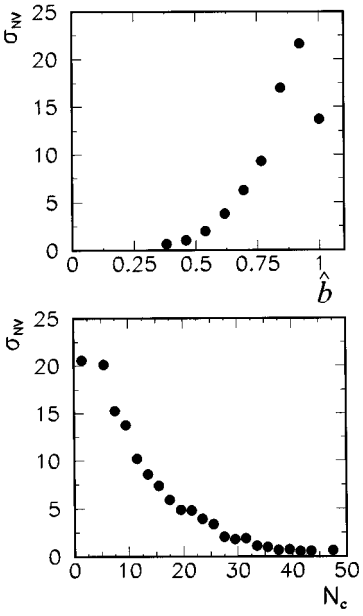


FIG. 10. Filtered CMD results. The normalized variance of the size of the largest fragment $\sigma_{\rm NV}$ vs the reduced impact parameter $\hat{b}$ (upper panel) and vs charged particle multiplicity $N_c$ (lower panel).

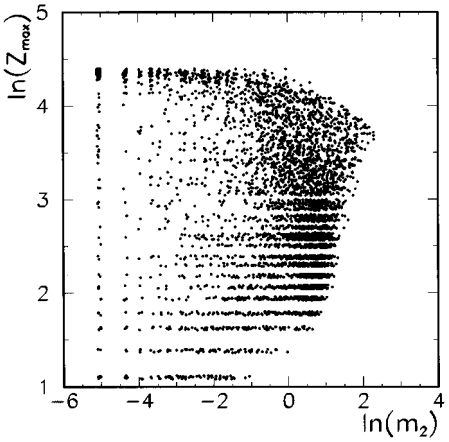


FIG. 11. Filtered CMD results. Campi scatter plot. The logarithm of the size of the largest fragment $\ln(Z_{\max})$ is plotted vs the logarithm of the second moment $\ln(m_2)$.

size of the largest fragment, the characteristic shape of the Campi scatter plot and the occurrence of large fluctuations in the region of the Campi plot where the critical behavior is expected.

## IV. EFFECTS OF EXPERIMENTAL INEFFICIENCY

As indicated in the Introduction, one of the aims of this study is to apply the same procedure of critical behavior identification to the experimental data obtained by the MULTICS-MINIBALL Collaboration for the same reaction, Au + Au at 35 MeV/nucleon. To do so, we have filtered our results using the angular acceptance and energy thresholds of the MULTICS-MINIBALL apparatus.

We have checked that at least for semiperipheral and peripheral collisions, the efficiency of the apparatus automatically eliminates the largest fragment coming from the target-like, so we calculate the moments of charge distributions $m_k$ [Eq. (2)] by subtracting only the largest fragment (and not the two largest ones as for the unfiltered results). The upper part of Fig. 8 shows the second moment $m_2$ vs $\hat{b}$. The second moment $m_2$ no longer shows the peak observed for unfiltered results around $\hat{b}=0.8$, even though one notes some remaining of that peak. We note also the appearance of a bump for more central collisions, around $\hat{b}=0.38$. The situ-

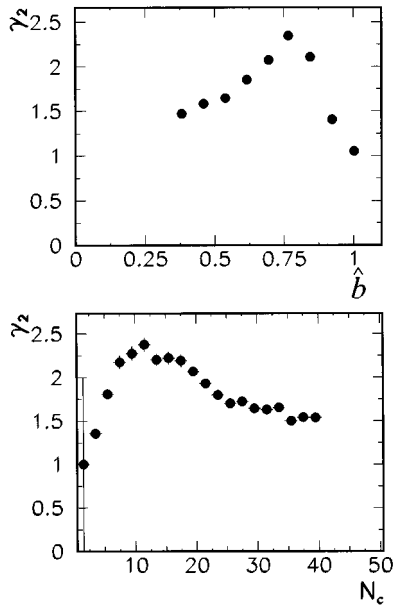


FIG. 13. Filtered CMD results with selection of events. The reduced variance $\gamma_2$ vs the reduced impact parameter $\hat{b}$ (upper panel) and vs charged particle multiplicity $N_c$ (lower panel).

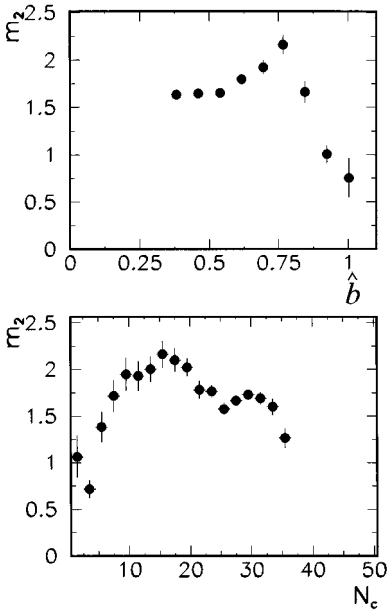


FIG. 12. Filtered CMD results with selection of events. The second moment of charge distributions $m_2$ vs the reduced impact parameter $\hat{b}$ (upper panel) and vs charged particle multiplicity $N_c$ (lower panel).

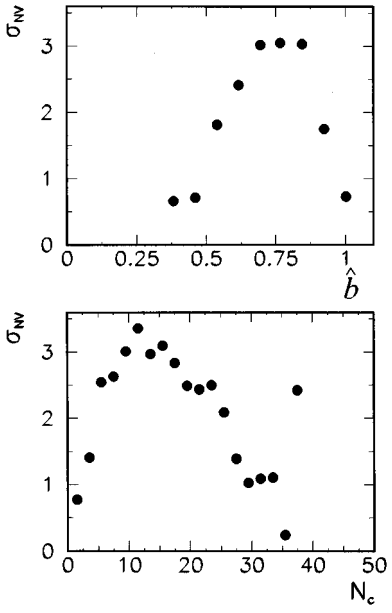


FIG. 14. Filtered CMD results with selection of events. The normalized variance of the size of the largest fragment $\sigma_{\mathrm{NV}}$ vs the reduced impact parameter $\hat{b}$ (upper panel) and vs charged particle multiplicity $N_c$ (lower panel).

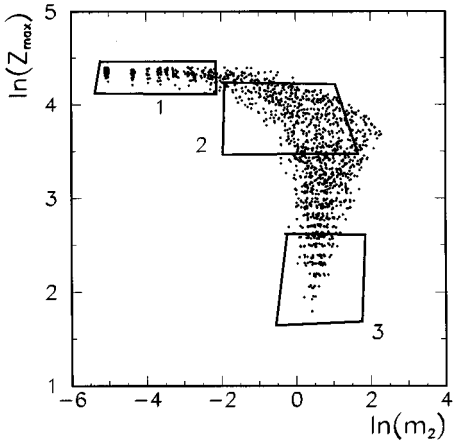


FIG. 15. Filtered CMD results with selection of events. Campi scatter plot. The logarithm of the size of the largest fragment $\ln(Z_{max})$ is plotted vs the logarithm of the second moment $\ln(m_2)$. Three cuts are employed to select the upper branch (1), the lower branch (3), and the central region (2).

ation is worst for the plot of $m_2$ vs $N_c$ in the lower panel of the figure where one observes only a quasilinear rise. The reduced variance $\gamma_2$ drawn in Fig. 9, shows a bit different behavior. One still observes a smooth bump at $\hat{b}=0.8$ but $\gamma_2$ is almost constant for $\hat{b}<0.8$ and not rising as it is the case for unfiltered results. Similarly for $\gamma_2$ vs $N_c$, lower part of Fig. 9. The normalized variance of the size of the largest fragment given in Fig. 10, still shows a peak but slightly shifted towards higher impact parameters (upper part of the figure, compare to Fig. 4) or shifted towards lower charged particle multiplicity (lower part of Fig. 10). More drastic is the change in the shape of the Campi scatter plot shown in Fig. 11. This plot no longer shows any particular shape characteristic of the occurrence of a critical behavior (observed in the unfiltered results) and one is no more able to identify the upper and lower branches neither the meeting zone.

The effects of apparatus inefficiencies can thus be more or less drastic depending on the variable we are looking at. To recover the signals of criticality, we adopted the following procedure.

(i) Since the critical behavior was observed at peripheral impact parameters, we identify semiperipheral and peripheral collisions, eliminating more central ones, by selecting those events in which the velocity of the largest fragment along the beam axis is larger or equal to 75% of the beam velocity, which means that we are selecting those events in which there is a remnant of the projectile flying with the velocity of the quasiprojectile. Doing this, we wish to select only those reactions where two or three primary sources are formed (semiperipheral and peripheral reactions) and eliminate the reactions where only one source is formed at midrapidity (central collisions).

(ii) We select the most complete events imposing that the total detected charge is larger than 70 ($Z_{tot}\geqslant 70$).

Furthermore, we noted that condition (i) does not automatically eliminate all central collisions and in order to accomplish that we impose a maximum limit to the total detected charge, $Z_{tot}\leqslant 90-95$. We note also that changing condition (i) from 75% to 85% of the beam velocity for example does not change significantly the results, and only decreases the statistics.

In Figs. 12–14, we have plotted the second moment $m_2$, the reduced variance $\gamma_2$, and the normalized variance $\sigma_{NV}$ vs the reduced impact parameter $\hat{b}$ (upper part of the figures) and vs charged particle multiplicity $N_c$ (lower part). One sees that the signals observed for nonfiltered results are recovered at the same impact parameter. One notes also that this selection eliminates central collisions with $\hat{b}\leqslant 0.38$.

Figure 15 displays the Campi scatter plot for the filtered events with the selection on the velocity of the largest fragment and the total detected charge. We see that one recovers the characteristic shape of the Campi plot, i.e., an upper branch with a negative slope and a lower branch with a positive slope, already observed in the unfiltered results. To better clarify the characteristics of these two branches and of the

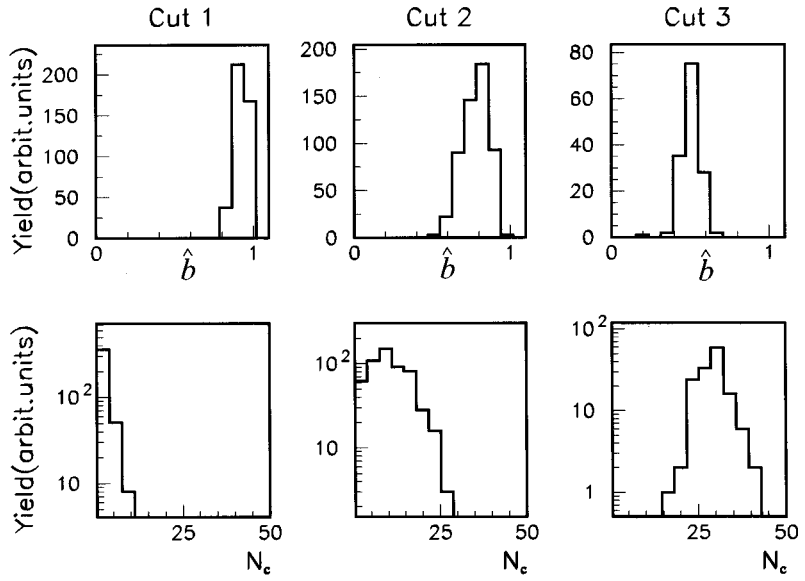


FIG. 16. Filtered CMD results with selection of events. Impact parameter distributions (upper panels) and multiplicity distributions (lower panels) for the three cuts made on Fig. 15: left part cut 1, central part cut 2, and right part cut 3.

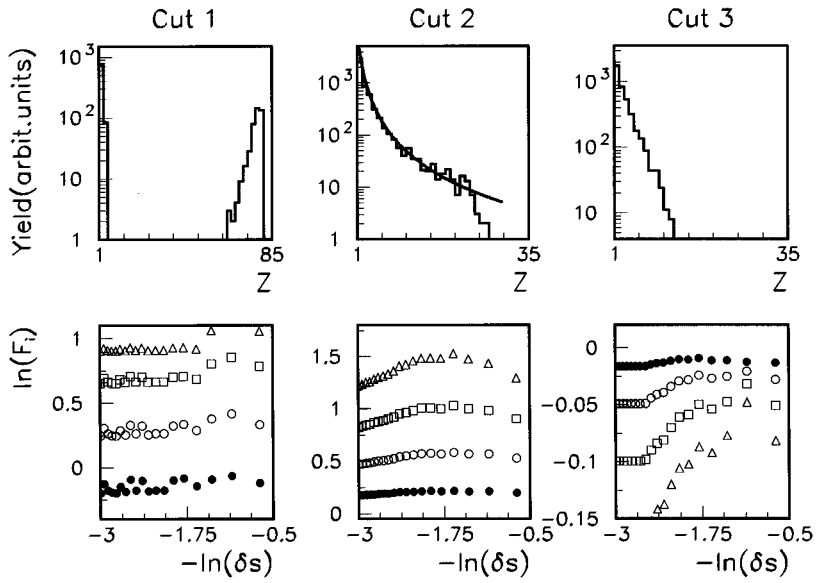


FIG. 17. Filtered CMD results with selection of events. Fragment charge distributions (upper panels) and the corresponding scaled factorial moments $\ln(F_i)$ vs $-\ln(\delta s)$ for the three cuts made on Fig. 15: left part cut 1, central part cut 2, and right part cut 3. The solid line on the upper-central panel indicates a power law distribution $N(Z)\propto Z^{-\tau}$ with $\tau=2.2$. In the lower panels, solid circles represent the SFM of order $i=2$, open circles $i=3$, open squares $i=4$, and open triangles $i=5$.

meeting zone, we have made three cuts in this plot selecting the upper branch (cut 1), the lower branch (cut 3), and the central region (cut 2), and analyzed the events falling in each of the three cuts. The upper part of Fig. 16 shows the impact parameter distributions of the events falling in the three cuts of the Campi plot. One sees that the three cuts select different regions of the impact parameter distribution: cut 1 (left panel) selects the most peripheral collisions with a distribution peaked at $\hat{b}=0.92$; cut 2 (central panel) selects peripheral impact parameters with a distribution going from $\hat{b}=0.65$ to 0.95; cut 3 (right panel) selects more central collisions. In the lower part of the same figure, we have plotted the charged particles multiplicity distributions for the three cuts. Cut 1 shows a multiplicity distribution from 2 to 10 while cut 3 shows a distribution at higher multiplicities from 30 to 45. The situation is different for cut 2. The multiplicity distribution covers a wider range of $N_c$ values from 2 to 30. Note that this large multiplicity distribution is not due, as one might think, to a large impact parameter mixing (see upper part of the figure), but is due to the occurrence of large fluctuations as expected near the critical point as we will show below.

Figure 17 displays in the upper part the fragment charge distributions obtained in the three cuts [36] with, in the lower part, the corresponding scaled factorial moments calculated according to Eq. (6) [36]. Cut 1 (left part of the figure) corresponds to undercritical events and hence one obtains a charge distribution with a ''*U*'' shape characteristic to evaporation events, while for cut 3 (right part) one observes a rapidly decreasing charge distribution with an exponential shape characteristic to highly excited systems going to vaporization. For cut 2 (central part), we obtain a fragment charge distribution exhibiting a power law $Z^{-\tau}$, with $\tau\approx 2.2$, which is expected, according to the droplet model of Fisher, for fragment formation near the critical point indicating a liquid-gas phase transition, and consistent with the scaling laws of critical exponents [10]. In the lower part of the figure, for region 1 corresponding to evaporation events, the logarithms of the scaled factorial moments $\ln(F_i)$ are always flat and independent on $-\ln(\delta s)$ and there is no intermittency signal. For cut 2 the situation is different. The logarithms of the SFM's are positive and almost linearly increasing vs $-\ln(\delta s)$ and a strong intermittency signal is observed [note the absolute values of $\ln(F_i)$]. Cut 3 gives negative logarithms of the SFM's and we have also in this case no intermittency signal. Note that this behavior of the scaled factorial moments is exactly the same as that observed in percolation and molecular dynamics models for undercritical, critical, and overcritical events, respectively [17,37].

## V. CONCLUSIONS AND OUTLOOKS

In conclusion, we have studied the reaction Au+Au at an incident energy of 35 MeV/nucleon within the framework of classical molecular dynamics. The results show evidence for the occurrence of a critical behavior revealed through the

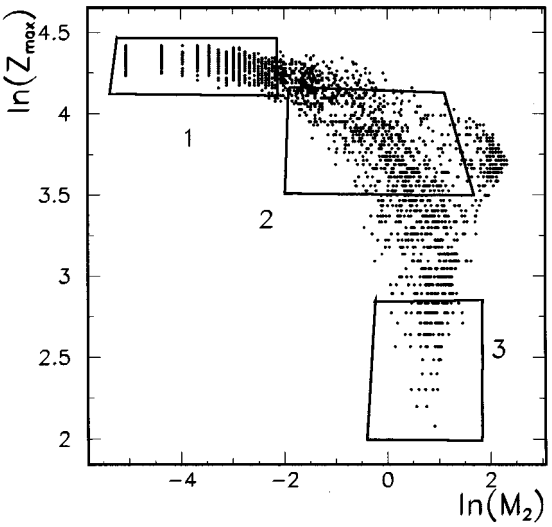


FIG. 18. Experimental results from Ref. [38]. Campi scatter plot. The logarithm of the size of the largest fragment $\ln(Z_{\max})$ is plotted vs the logarithm of the second moment $\ln(m_2)$. Three cuts are employed to select the upper branch (1), the lower branch (3), and the central region (2).

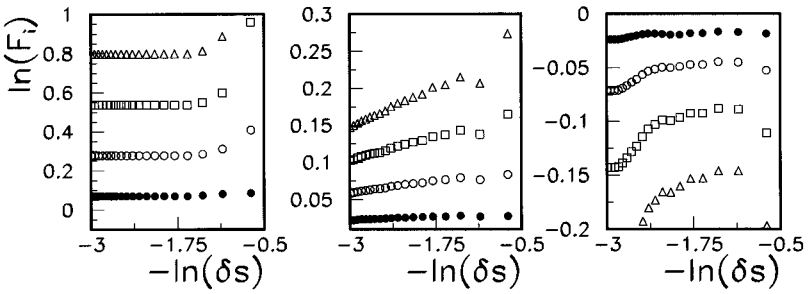


FIG. 19. Experimental results from Ref. [38]. Scaled factorial moments $\ln(F_i)$ vs $-\ln(\delta s)$ for the three cuts made on Fig. 18: left part cut 1, central part cut 2, and right part cut 3. Solid circles represent the SFM of order $i=2$, open circles $i=3$, open squares $i=4$, and open triangles $i=5$.

shape of the second moment of charge distributions, the reduced variance, the normalized variance of the size of the largest fragment, the particular shape of the Campi scatter plot and through the presence of large fluctuations as indicated by the intermittency analysis in the region of the Campi plot where the critical behavior is expected. We have also seen that when our results are filtered using the geometrical acceptance and energy thresholds of the MULTICS-MINIBALL apparatus, experimental inefficiencies can hide more or less the signals of criticality. Moreover, we have shown that these criticality signals can be recovered by identifying the most complete semiperipheral and peripheral events selecting those events in which the largest fragment has a velocity along the beam axis larger or equal to 75% of the beam velocity and for which the total detected charge is $70 \leqslant Z_{\mathrm{tot}} \leqslant 90$.

We would like to note at the end that the same procedure for characterizing the critical behavior has been successfully applied to the experimental data obtained by the MULTICS-MINIBALL Collaboration for the same reaction Au + Au at 35 MeV/nucleon, and that a critical behavior has been identified [38]. As an example, we show in Fig. 18 the experimental Campi scatter plot [38] obtained making a similar event selection as for the CMD results. Note the strong similarity with the theoretical Campi plot shown in Fig. 15. Moreover, we show in Fig. 19 the experimental scaled factorial moments [38] obtained in the three cuts made on the Campi plot of Fig. 18. Once again note the similarity of these results with those of the CMD results. The authors of the previous reference have also extracted the other quantities discussed in this paper (variance of the charge of the largest fragment, etc.) from the experimental data [39]. These quantities behave very similarly to what is discussed here for the CMD case thus strengthening our findings. A very similar behavior to the one discussed here has also recently been observed in Xe + Sn collisions at 55 MeV/nucleon measured with the detector INDRA again for peripheral collisions [40]. Work now is in progress to characterize the fragmenting sources leading to the critical behavior and to extract the critical exponents.

## ACKNOWLEDGMENTS

One of us (M. Belkacem) thanks the Physics Department of the University of Trieste for financial support and the Physics Department of the University of Bologna, where part of this work was done, for warm hospitality and financial support.

[1] M. W. Curtain, H. Toki, and D. K. Scott, Phys. Lett. **123B**, 289 (1983); A. D. Panagiotou, M. W. Curtain, H. Toki, D. K. Scott, and P. J. Siemens, Phys. Rev. Lett. **52**, 496 (1984).

[2] G. F. Bertsch and P. J. Siemens, Phys. Lett. **126B**, 9 (1983).

[3] A. L. Goodman, J. I. Kapusta, and A. Z. Mekjian, Phys. Rev. C **30**, 851 (1984).

[4] H. R. Jaqaman, Gabor Papp, and D. H. E. Gross, Nucl. Phys. **A514**, 327 (1990).

[5] R. G. Palmer and P. W. Anderson, Phys. Rev. D **9**, 3281 (1974); W. G. Kupper, G. Wegmann, and E. R. Hilf, Ann. Phys. **88**, 454 (1974); G. Sauer, H. Chandra, and U. Mosel, Nucl. Phys. **A264**, 221 (1976).

[6] P. Danielewicz, Nucl. Phys. **A314**, 465 (1979).

[7] D. Q. Lamb, J. M. Lattimer, C. J. Pethick, and D. G. Ravenhall, Phys. Lett. **41**, 1623 (1978); Nucl. Phys. **A360**, 459 (1981); H. Schulz, L. Münchow, G. Röpke, and M. Schmidt, Phys. Lett. **119B**, 12 (1982); Nucl. Phys. **A399**, 587 (1983).

[8] H. R. Jaqaman, A. Z. Mekjian, and L. Zamick, Phys. Rev. C **27**, 2782 (1983); **29**, 2067 (1984).

[9] J. E. Finn *et al.*, Phys. Rev. Lett. **49**, 1321 (1982); Phys. Lett. **118B**, 458 (1982); H. H. Gutbrod, A. I. Warwick, and H. Wieman, Nucl. Phys. **A387**, 177c (1982); M. Mahi, A. T. Bujak, D. D. Carmony, Y. H. Chung, L. J. Gutay, A. S. Hirsch, G. L. Paderewski, N. T. Porile, T. C. Sangster, R. P. Scharenberg, and B. C. Stringfellow, Phys. Rev. Lett. **60**, 1936 (1988).

[10] M. E. Fisher, Rep. Prog. Phys. **30**, 615 (1967); in *Proceedings of the International School of Physics*, Enrico Fermi Course LI, Critical Phenomena, edited by M. S. Green (Academic, New York, 1971); Physics **3**, 255 (1967).

[11] J. B. Elliott, M. L. Gilkes, J. A. Hauger, A. S. Hirsch, E. Hjort, N. T. Porile, R. P. Scharenberg, B. K. Srivastava, M. L. Tincknell, and P. G. Warren, Phys. Rev. C **49**, 3185 (1994); M. L. Gilkes *et al.*, Phys. Rev. Lett. **73**, 1590 (1994).

[12] J. Pochodzalla *et al.*, Phys. Rev. Lett. **75**, 1040 (1995).

[13] I. Iori *et al.*, Nucl. Instrum. Methods A **325**, 458 (1993).

[14] R. T. DeSouza *et al.*, Nucl. Instrum. Methods A **295**, 109 (1990).

[15] M. D'Agostino *et al.*, Phys. Rev. Lett. **75**, 4373 (1995); Phys. Lett. B **368**, 259 (1995).

[16] R. J. Lenk, T. J. Schlagel, and V. R. Pandharipande, Phys. Rev. C **42**, 372 (1990).

[17] V. Latora, M. Belkacem, and A. Bonasera, Phys. Rev. Lett. **73**

1765 (1994); M. Belkacem, V. Latora, and A. Bonasera, Phys. Rev. C **52**, 271 (1995).
[18] V. Latora, A. Del Zoppo, and A. Bonasera, Nucl. Phys. **A572**, 477 (1994).
[19] S. E. Koonin and D. C. Meredith, *Computational Physics* (Addison-Wesley, California, 1990).
[20] L. Wilet, E. M. Henley, M. Kraft, and A. D. MacKellar, Nucl. Phys. **A282**, 341 (1977); H. Horiuchi, *ibid.* **A522**, 257c (1991).
[21] D. H. E Gross, Prog. Nucl. Phys. **30**, 155 (1993); A. S. Botvina and D. H. E. Gross, Nucl. Phys. **A592**, 257 (1995).
[22] J. Bondorf *et al.*, Nucl. Phys. **A444**, 460 (1985); J. Bondorf, A. S. Botvina, A. S. Iljinov, I. N. Mishustin, and K. Sneppen, Phys. Rep. **257**, 133 (1995).
[23] A. Bonasera, F. Gulminelli, and J. Molitoris, Phys. Rep. **243**, 1 (1994).
[24] X. Campi, J. Phys. A **19**, L917 (1986); X. Campi, Phys. Lett. B **208**, 351 (1988); J. Phys. (Paris) **50**, 183 (1989).
[25] R. Balescu, *Equilibrium and Nonequilibrium Statistical Mechanics* (Krieger, Malabar, FL, 1991).
[26] P. Finocchiaro, M. Belkacem, T. Kubo, V. Latora, and A. Bonasera, Nucl. Phys. **A600**, 236 (1996).
[27] H. E. Stanley, *Introduction to Phase Transitions and Critical Phenomena* (Oxford University Press, Oxford, 1987).
[28] C. O. Dorso, M. Belkacem, V. Latora, and A. Bonasera (unpublished).
[29] H. R. Jaqaman and D. H. E. Gross, Nucl. Phys. **A524**, 321 (1991); D. H. E. Gross, A. R. DeAngelis, H. R. Jaqaman, Pan Jicai, and R. Heck, Phys. Rev. Lett. **68**, 146 (1992); A. R. DeAngelis, D. H. E. Gross, and R. Heck, Nucl. Phys. **A537**, 606 (1992).
[30] A. Bialas and R. Peschanski, Nucl. Phys. **B273**, 703 (1986); **B308**, 857 (1988).
[31] M. Ploszajczak and A. Tucholski, Phys. Rev. Lett. **65**, 1539 (1990); Nucl. Phys. **A523**, 651 (1991).
[32] X. Campi and H. Krivine, Nucl. Phys. **A589**, 505 (1995).
[33] L. Phair *et al.*, Phys. Lett. B **291**, 7 (1992).
[34] R. C. Hwa and M. T. Nazirov, Phys. Rev. Lett. **69**, 741 (1992).
[35] T. Kubo, M. Belkacem, V. Latora, and A. Bonasera, Z. Phys. A **352**, 145 (1995).
[36] Charge distributions and the SFM shown in Fig. 17 have been calculated without the heaviest fragment in each event, apart the charge distribution of cut 1.
[37] M. Baldo, A. Causa, and A. Rapisarda, Phys. Rev. C **48**, 2520 (1993).
[38] P. F. Mastinu *et al.*, Phys. Rev. Lett. **76**, 2646 (1996).
[39] P. F. Mastinu, in *Proceedings of the XXXIV International Winter Meeting on Nuclear Physics*, Bornio, 1996, edited by I. Iori [Ric. Sci. E.P. **102**, 110 (1996)].
[40] J. Benlliure, Ph.D. thesis, University of Valencia, Spain, 1995.